

## DEVELOPMENT

# Axis formation in annual killifish: Nodal and $\beta$ -catenin regulate morphogenesis without Huluwa prepatternning

Philip B. Abitua<sup>1,2\*</sup>, Laura M. Stump<sup>1,†</sup>, Deniz C. Aksel<sup>3,†</sup>, Alexander F. Schier<sup>2,4,5,6,7,8</sup>

Axis formation in fish and amphibians typically begins with a prepattern of maternal gene products. Annual killifish embryogenesis, however, challenges prepatternning models as blastomeres disperse and then aggregate to form the germ layers and body axes. We show that *huluwa*, a prepatternning factor thought to break symmetry by stabilizing  $\beta$ -catenin, is truncated and inactive in *Nothobranchius furzeri*. Nuclear  $\beta$ -catenin is not selectively stabilized on one side of the blastula but accumulates in cells forming the aggregate. Blocking  $\beta$ -catenin activity or Nodal signaling disrupts aggregate formation and germ layer specification. Nodal signaling coordinates cell migration, establishing an early role for this signaling pathway. These results reveal a surprising departure from established mechanisms of axis formation: Huluwa-mediated prepatternning is dispensable, and  $\beta$ -catenin and Nodal regulate morphogenesis.

A century ago, Spemann and Mangold reported that cells on the dorsal side of gastrulating newt embryos could induce a secondary axis when transplanted into the ventral side of a host embryo (1). They named this group of cells the “organizer” for its ability to organize surrounding tissue into a separate body axis. It is believed that anamniotes (i.e., fishes and amphibians) generate the organizer by breaking radial symmetry through a prepattern of maternally provided mRNAs. In particular, the maternal determinant *huluwa* is partitioned to the future dorsal side, culminating in the stabilization and nuclear accumulation of  $\beta$ -catenin, which acts as a transcriptional activator of organizer-specific genes (2). After dorsal-ventral axis determination, the transforming growth factor- $\beta$  morphogen Nodal induces the phosphorylation of the downstream effector Smad2, resulting in mesoderm and endoderm specification (3).

Among teleosts, annual killifish have an atypical development that challenges current models of axis formation (4). Although the cells of the extra-embryonic enveloping layer (EVL) expand over the surface of the yolk as in conventional epiboly, the deep blastomeres completely disperse and only aggregate later to form the embryo proper (Fig. 1A). At the onset of epiboly these blastomeres de-adhere from one another and spread across the ex-

panding EVL through “contact inhibition of locomotion,” a phenomenon in which cells change their direction upon collision with one another (5, 6). At the end of epiboly, the deep cells of annual killifish are completely dispersed as single cells (4). By contrast, blastomeres in other teleosts, such as zebrafish and medaka, stay adherent and intercalate (3, 7). The dispersion of deep blastomeres raises the question of whether prepatternning is involved in axis specification and how Huluwa,  $\beta$ -catenin, and Nodal act in annual killifish. To address these questions, we chose the annual killifish *Nothobranchius furzeri* as a model system, owing to its genetic tractability and available reference genome (8–10).

## Nodal and $\beta$ -catenin activity during the early embryogenesis of *N. furzeri*

To understand how the embryonic axes form in *N. furzeri*, we analyzed the expression of marker genes, performed timelapse imaging, and studied the activity of the Huluwa/ $\beta$ -catenin and Nodal pathways. We first sought to visualize when and where  $\beta$ -catenin was stabilized during *N. furzeri* development. Using a  $\beta$ -catenin antibody against zebrafish Ctnnb1, we observed uniform  $\beta$ -catenin nuclear localization prior to dispersion (256-cell stage) (fig. S1A), in contrast to the asymmetric localization observed in other anamniotes (11, 12). During the dispersed phase,  $\beta$ -catenin staining was markedly reduced (fig. S1B). Nuclear  $\beta$ -catenin accumulated again in a cluster of cells that formed the incipient aggregate (fig. S1C, below the dashed line). As aggregation continued, nuclear  $\beta$ -catenin was largely restricted to peripheral cells that were in the process of joining the aggregate (fig. S1D, above the dashed line).

To directly monitor  $\beta$ -catenin dynamics in live embryos, we generated a transgenic line that expressed a fluorescently tagged nano-

body that binds to  $\beta$ -catenin (13). Live imaging showed a decrease in  $\beta$ -catenin levels as cells dispersed, consistent with the observations made with the  $\beta$ -catenin antibody (Fig. 1B, fig. S1B, and movie S1). During incipient aggregation,  $\beta$ -catenin was seen accumulating in the nuclei of a cluster of individual cells that subsequently formed the center of the future aggregate (Fig. 1C, fig. S1C, and movie S2). Notably, the accumulation of nuclear  $\beta$ -catenin was dynamic as cells near the future aggregate only transiently accumulated nuclear signal (fig. S2 and movie S2). Eventually the nuclear  $\beta$ -catenin signal stabilized in the incipient aggregate as cells adhered to each other (Fig. 1C and fig. S2). The absence of a stable pattern before the formation of the incipient aggregate suggests that  $\beta$ -catenin is not regulated by maternal dorsal determinants in the early blastula of *N. furzeri*. Instead, its later accumulation marks the site of aggregation.

We next asked whether Nodal signaling also differs between *N. furzeri* and other anamniotes. In zebrafish, Nodal gene expression and pathway activity are found at the blastula margin and then become restricted to the axial mesoderm (14). By contrast, the *N. furzeri* Nodal gene *ndr2* showed broad and weak early expression in deep cells during the dispersed phase (Fig. 2A). At the incipient aggregate stage, *ndr2* expression was enriched in a cluster of cells where cell-cell adhesion had initiated (Fig. 2B). The timing and location of *ndr2* expression correlated with the emergence of nuclear  $\beta$ -catenin in the incipient aggregate (Fig. 1C). As cells continued to join the early aggregate, *ndr2* expression and nuclear Smad2 staining also were strongest in the aggregate center (Fig. 2, C and D). *Lefty1*, a Nodal feedback inhibitor (3), was also expressed in a cluster of deep cells at the site of the incipient aggregate (Fig. 2E). Thus, in contrast to zebrafish, *N. furzeri* Nodal is initially broadly expressed and then becomes restricted to the center of the aggregate.

The emergence of a spatial pattern in gene expression during the incipient aggregate stage is also reflected in the expression of other marker genes. The expression of *pou5f3*, a marker of pluripotency, decreased during the dispersed phase in deep blastomeres (fig. S3, A to C), whereas *chordin*, a bone morphogenetic protein antagonist secreted from the dorsal organizer of vertebrates, became expressed in the incipient aggregate (Fig. 2F). This site of the future aggregate also expressed the mesodermal marker genes *tbx4a* and *tbx6l* (Fig. 2G and fig. S4, A to C). Notably, *sox2*, a well-known ectoderm marker, was not expressed at this stage, unlike in zebrafish (15) (fig. S4D). Together, these results indicate that the incipient aggregate of *N. furzeri* corresponds to the dorsal organizer and presumptive mesoderm and is the site of high  $\beta$ -catenin and Nodal signaling activity, similar to other anamniotes.

<sup>1</sup>Genome Sciences, University of Washington, Seattle, WA 98105, USA. <sup>2</sup>Department of Molecular and Cellular Biology, Harvard University, Cambridge, MA 02138, USA. <sup>3</sup>Biophysics Program, Harvard University, Cambridge, MA 02138, USA.

<sup>4</sup>Broad Institute of MIT and Harvard, Cambridge, MA 02142, USA. <sup>5</sup>Center for Brain Science, Harvard University, Cambridge, MA 02138, USA. <sup>6</sup>FAS Center for Systems Biology, Harvard University, Cambridge, MA 02138, USA.

<sup>7</sup>Biozentrum, University of Basel, 4051 Basel, Switzerland.

<sup>8</sup>Allen Discovery Center for Cell Lineage Tracing, University of Washington, Seattle, WA 98195, USA.

\*Corresponding author. Email: abitua@uw.edu

†These authors contributed equally to this work.

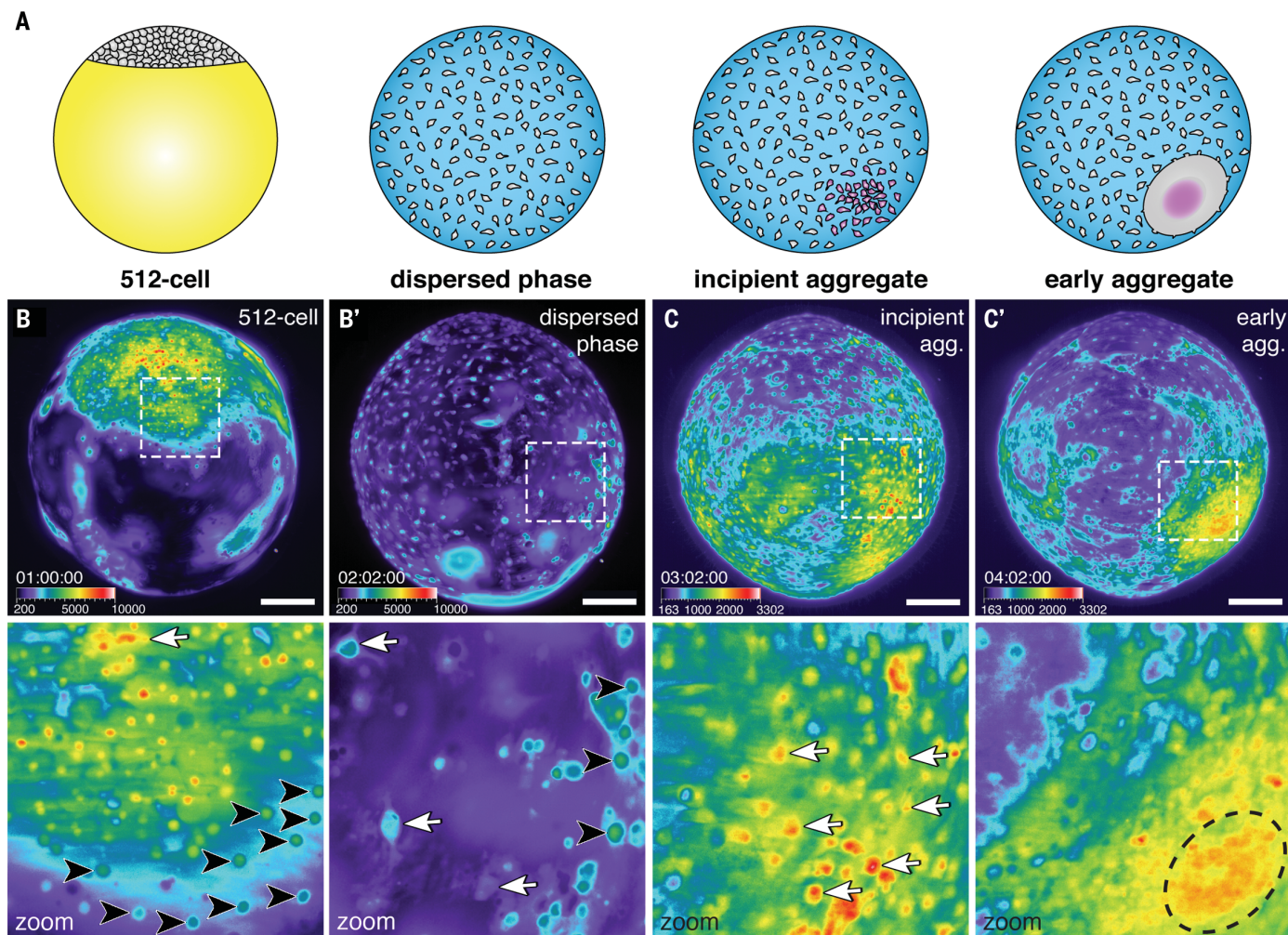


**Fig. 1. Nuclear  $\beta$ -catenin dynamics during early *N. furzeri* development.**

(A) Schematic of *N. furzeri* stages. Yellow represents the yolk not yet enveloped by the EVL, and magenta represents the mesoderm. Animal pole is up. (B) Snapshots from a timelapse of transgenic BC1:egfp embryo starting at approximately the 512-cell stage during the onset of dispersion. (B') View at the end of epiboly. (C) Snapshots from a timelapse of transgenic BC1:egfp embryo starting at the

incipient aggregate stage. (C') View during early aggregate stage, 24 hours later. White boxes in (B) and (C) indicate the regions for the zoomed-in view in the panels below, highlighting EVL (black arrowheads) and deep cells (white arrows). The black dashed circle indicates center of early aggregate. All images are lateral views. Timestamp indicates days, hours, and minutes starting from fertilization. The signal intensity is color coded (see intensity scale). Scale bars, 200  $\mu$ m.

#### Axis formation in *N. furzeri*

As development proceeds, germ layer marker gene expression also becomes more similar to other teleosts. Future ectodermal cells joined the aggregate and surrounded the presumptive mesoderm, which then internalized to define the body axes (fig. S4). In the early aggregate, prior to gastrulation, presumptive axial mesoderm expressing *tbx1a* was situated at the center of *tbx6l*-expressing paraxial mesoderm (fig. S4, F and G). During this stage, *sox2* was weakly expressed at the edge peripheral to the mesoderm in the presumptive ectoderm (fig. S4H). At the bud stage, these patterns were further refined into discrete domains: *Lefty1* was expressed throughout the entire axial mesoderm and *tbx1a* was specifically expressed in the ingressing posterior axial mesoderm, whereas *tbx6l* was restricted to the flanking paraxial

mesoderm (fig. S4, I to L). The ectodermal marker *sox2* was expressed in the surface ectoderm and was absent from the mesodermal tissue (fig. S4, M and P). The ectoderm was subdivided along the anterior-posterior axis as evidenced by the expression of *otx2b* and *gbx1* (fig. S4, N and O). Despite the unusual early morphogenesis in which deep cells dispersed, migrated, and then aggregated, by the 10-somite stage *N. furzeri* expression patterns were typical for teleosts, including for a related annual killifish of the genus *Austrolebias* (fig. S4, Q to T) (6, 14–16).

To capture the process of axis formation we used light sheet microscopy starting from the incipient aggregate stage until the onset of the pharyngula period (movie S3). The incipient aggregate expanded in size through progressive condensation of deep cells in the vegetal hemisphere of the embryo until approximately

84 hours postfertilization (hpf) (fig. S5, A and B). Afterward, gastrulation initiated and the axial mesoderm ingressed, causing the axis to extend anteriorly until the embryo reached the bud stage at about 96 hpf (fig. S5C). Subsequently at around 100 hpf, segmentation began (fig. S5D) and advanced to the 10-somite stage by approximately 120 hpf (fig. S5E). During the pharyngula period, the axis continued elongating, vasculature formed, and the heart tube extended anteriorly beyond the head (fig. S5F). At this point, on day 6 the *N. furzeri* embryos reached the phytotypic stage, despite atypical morphogenesis preceding gastrulation.

#### The prepatterning factor *Huluwa* is truncated

The absence of a clear pattern prior to aggregation led us to analyze the role of *huluwa* in *N. furzeri* axis formation. We identified

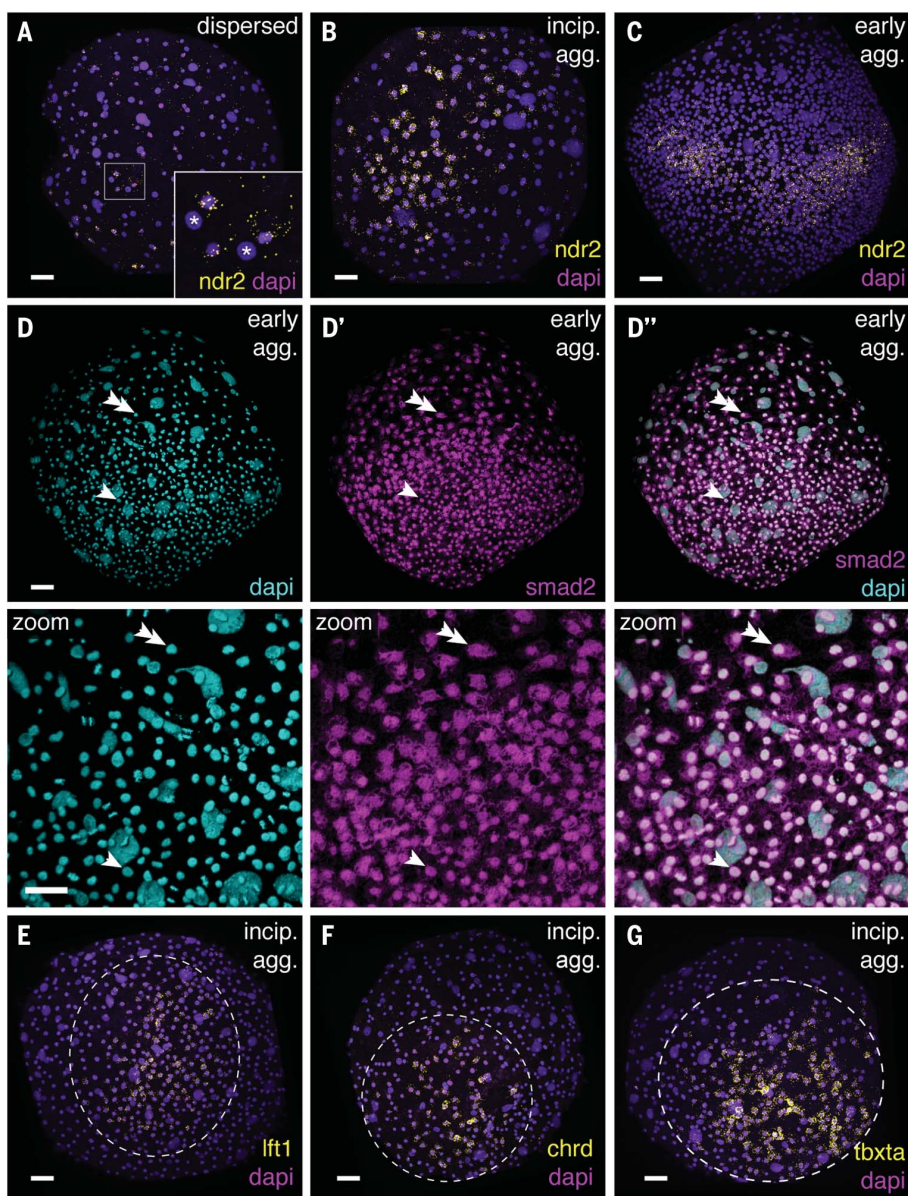


**Fig. 2. Pattern formation during *N. furzeri* development.** (A) *Ndr2* mRNA expression during the dispersed phase. Inset shows zoomed-in view of boxed area. Asterisks indicate EVL cells that lack *ndr2* mRNA. (B) *Ndr2* mRNA expression during the incipient aggregate stage. (C) *Ndr2* mRNA expression during the early aggregate stage. (D) Smad2 shows nuclear localization closer to the center of aggregated deep cells (compare arrowhead to double arrowhead). Zoomed-in view shows the periphery of the aggregate, which is positioned at the bottom. (E) *Lefty1* mRNA expression. (F) *Chordin* mRNA expression, and (G) *Tbxata* mRNA expression during the incipient aggregate stage. Dashed line demarcates the area of expression in (E) to (G). (A) to (C) and (E) to (G) aggregate views; (B) lateral aggregate view. Scale bars, 50  $\mu$ m.

the *N. furzeri huluwa* ortholog on chromosome Sgr02. Notably, aligning the genomic sequence of *N. furzeri huluwa* with other teleosts—including the closely related nonannual mangrove killifish, *Kryptolebias marmoratus*—revealed a single base pair insertion that results in a predicted frameshift mutation (Fig. 3A). Alignment of *N. furzeri huluwa* mRNA with other *huluwa* orthologs revealed that the predicted *N. furzeri* sequence was truncated, lacking the

conserved and essential C-terminal intracellular domain (Fig. 3, B and C) (2). These findings indicate that *N. furzeri huluwa* degenerated into a truncated protein.

To directly compare the activities of *N. furzeri huluwa* to its orthologs, we misexpressed *huluwa* from *N. furzeri*, zebrafish, and *K. marmoratus* by mRNA injection into one-cell zebrafish zygotes. Embryos misexpressing zebrafish and *K. marmoratus huluwa* had the ovoidal mor-

phology of dorsalized embryos (17) and died during segmentation (Fig. 3, D to G). By contrast, *N. furzeri huluwa* induced cell division defects but had no dorsalizing activity (Fig. 3E). These results indicate that *N. furzeri huluwa* is nonfunctional as a dorsalizing determinant.

#### **$\beta$ -catenin activity and Nodal signaling are required for aggregation**

The truncation of Huluwa and the dynamic accumulation of  $\beta$ -catenin prompted us to test the roles of  $\beta$ -catenin during axis formation. We treated dispersion phase embryos with iCRT14, a small molecule that blocks the interaction between  $\beta$ -catenin and T cell factor (TCF), thereby suppressing downstream transcriptional activity (Fig. 4A) (18). Notably, iCRT14 prevented aggregation and expression of germ layer markers (Fig. 4, B and C and E to H). By contrast, earlier treatment with iCRT14 from the one-cell stage to the dispersion phase did not prevent aggregation and only caused a slight delay in axis formation (Fig. 4D). Wild-type (WT) embryos formed axes and exhibited the expected expression patterns for *sox2* and *tbxta* at the 10-somite stage whereas iCRT14-treated embryos remained in the dispersed phase and failed to express either marker gene (Fig. 4 E to H). Conversely, treatment with LY2090314—a glycogen synthase kinase-3 (GSK-3) inhibitor that stabilizes  $\beta$ -catenin (19)—just before aggregation led to multiple and malformed aggregates (fig. S6). Altogether, these results reveal a pivotal role for  $\beta$ -catenin activity in aggregation and germ layer specification.

Given the importance of Nodal signaling in other systems, we next investigated whether Nodal was also crucial for aggregation. We incubated dispersion phase embryos in A-83-01, a selective inhibitor of Activin/Nodal type 1 receptors (20), or injected mRNA for the Nodal inhibitor *lefty1* at the one-cell stage. Initial cleavage divisions and epiboly were not affected (Fig. 5, A to C), but notably, inhibiting Nodal signaling completely blocked aggregation. Nodal-inhibited embryos failed to express the mesodermal markers *ndr2*, *lefty1*, *chordin*, and *tbxta* (fig. S7) as well as the ectodermal markers *sox2* and *otx2b* (fig. S3, E to H). Notably, *pou5f3* displayed similar expression in untreated dispersion phase embryos and Nodal-inhibited embryos that failed to aggregate (fig. S3, B and D). These results indicate that Nodal inhibition prevents aggregation and germ layer specification.

#### **Nodal signaling coordinates cell migration**

To perform detailed phenotypic analysis of the aggregation defect caused by Nodal inhibition, we used light sheet microscopy from the dispersed phase until axis formation in transgenic *N. furzeri* expressing a nuclear fluorescent marker (movies S4 and S5). Using an automated three-dimensional (3D) cell-tracking

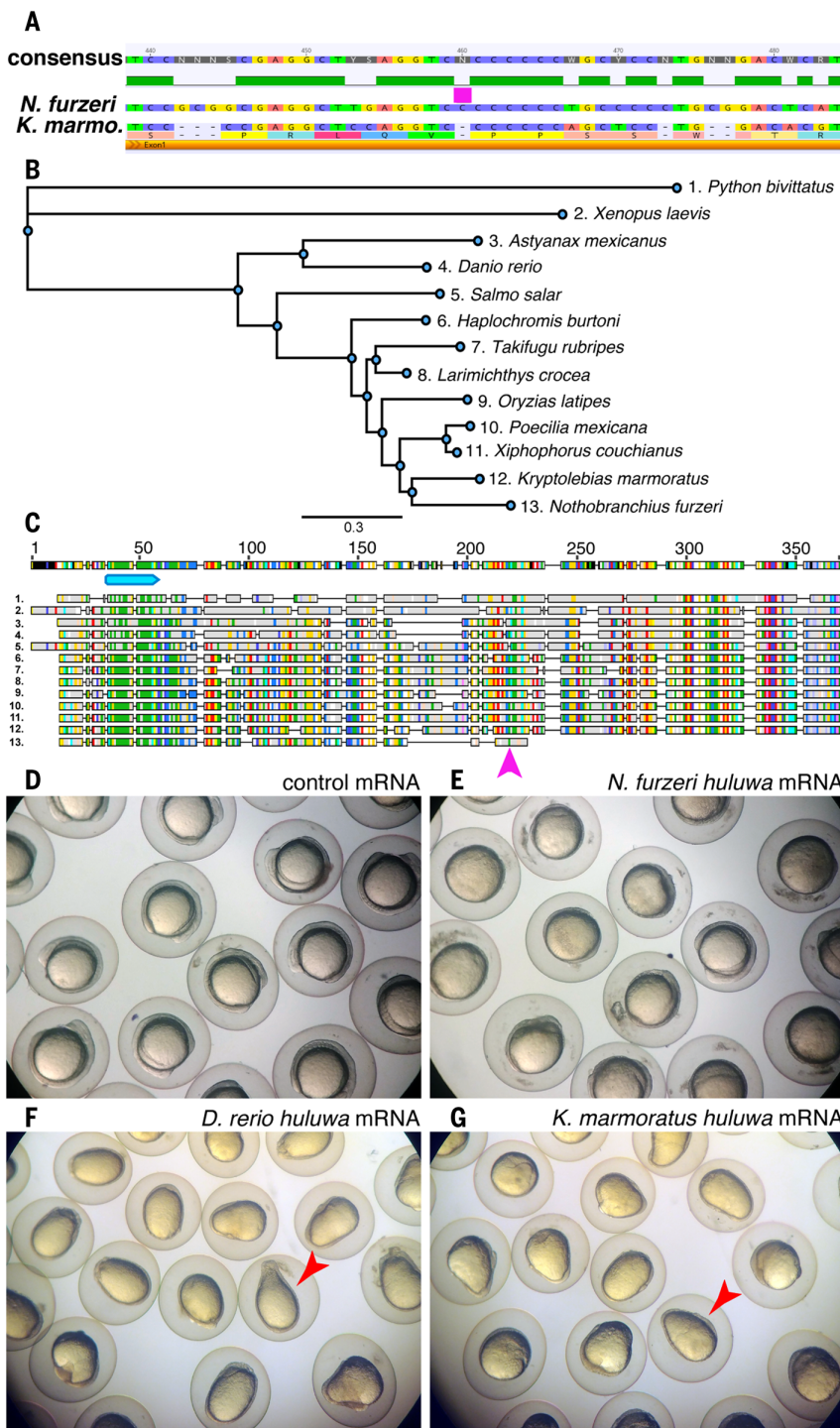


**Fig. 3. *N. furzeri* huluwa pseudogene lacks dorsalizing activity.** (A) Alignment of genomic sequences for *N. furzeri* and *K. marmoratus* huluwa. Magenta bar indicates the single base pair insertion in the *N. furzeri* sequence. (B) Phylogenetic tree of Huluwa orthologous proteins in 13 anamniote species. (C) Alignment of Huluwa orthologous proteins. Numbers correspond to the species indicated in (B). Amino acids are colored using the RasMol scheme. Cyan bar indicates the conserved transmembrane domain. Magenta arrow indicates the site of the frameshift mutation in the *N. furzeri* huluwa sequence (#13). (D) Embryos injected with 50 pg of control mRNA at the one-cell stage (0% severely dorsalized,  $n = 91$ ). (E) Embryos injected with 50 pg of *N. furzeri* huluwa mRNA at the one-cell stage (0% severely dorsalized,  $n = 84$ ). (F) Embryos injected with 50 pg of *D. rerio* huluwa mRNA at the one-cell stage (94.6% severely dorsalized,  $n = 92$ ). (G) Embryos injected with 50 pg of *K. marmoratus* huluwa mRNA at the one-cell stage (95.4% severely dorsalized,  $n = 107$ ). Red arrowheads in (F) and (G) indicate embryos with an ovoidal morphology, indicative of severe dorsalization. Images of embryos in (D) to (G) were acquired at the six-somite stage.

pipeline (27), we generated cell trajectories of individual blastomeres for WT and Nodal-inhibited embryos (Fig. 5, D and E, and fig. S8). By comparing cell behaviors (e.g., distributions of instantaneous speeds, persistence indices, and velocity autocorrelation decay times), we found that general motility was not affected by Nodal inhibition (Fig. 5, F and G, and fig. S8F). Next, we asked whether the local alignment and directionality of blastomeres was dependent on Nodal signaling. In the WT embryo, cell trajectories were on average more locally aligned, and mean cell directionalities pointed toward the aggregate (Fig. 5H). By contrast, cell trajectories were less aligned in the Nodal-inhibited embryo and directionalities were random (Fig. 5I). These results reveal that Nodal signaling in *N. furzeri* does not affect the motility of individual deep cells but is important for coordinated migration and aggregation.

#### Concluding remarks

Our results reveal four surprising divergences of early axis formation mechanisms in the annual killifish *N. furzeri* as compared to classically studied anamniotes: First, Huluwa is truncated and inactive as a dorsalizing determinant. Second, embryonic axis formation only emerges when  $\beta$ -catenin stabilizes during aggregation. Third,  $\beta$ -catenin activity is essential for aggregation. Fourth, Nodal signaling is required for coordinating cell migration and aggregation. Thus, in the absence of Huluwa-dependent prepatterning,  $\beta$ -catenin activity and Nodal-coordinated migration allow aggregation and subsequent axis formation.

What are the conserved or divergent aspects of *N. furzeri* embryogenesis? Some of the later features of pattern formation appear conserved between *N. furzeri*, zebrafish, and other fishes (6, 22). For example, *N. furzeri*  $\beta$ -catenin and *chordin* mark the dorsal organizer, and Nodal signaling and *tbx6* mark the presumptive mesoderm at the incipient aggregate stage. By contrast, at the blastula stage *N. furzeri* Huluwa is inactive as a dorsal determinant and  $\beta$ -catenin does not accumulate asymmetrically. *N. furzeri* Nodal signaling has maintained its conserved role in the activation of organizer and mesoderm genes, but notably it is also required for the directional migration and aggregation of the dispersed blastomeres. Nodal signaling has been implicated in tissue internalization, convergence, and elongation during gastrulation (23–27), but the much earlier role in *N. furzeri* raises the question of how Nodal signaling regulates the migration of dispersed cells, either directly or indirectly.

Why does the annual killifish *N. furzeri* use such a divergent strategy of axis formation? In the wild, the dispersed phase is often prolonged by the entry into diapause I, a suspended state that allows survival during the dry season. There are at least three possibilities why this dispersed

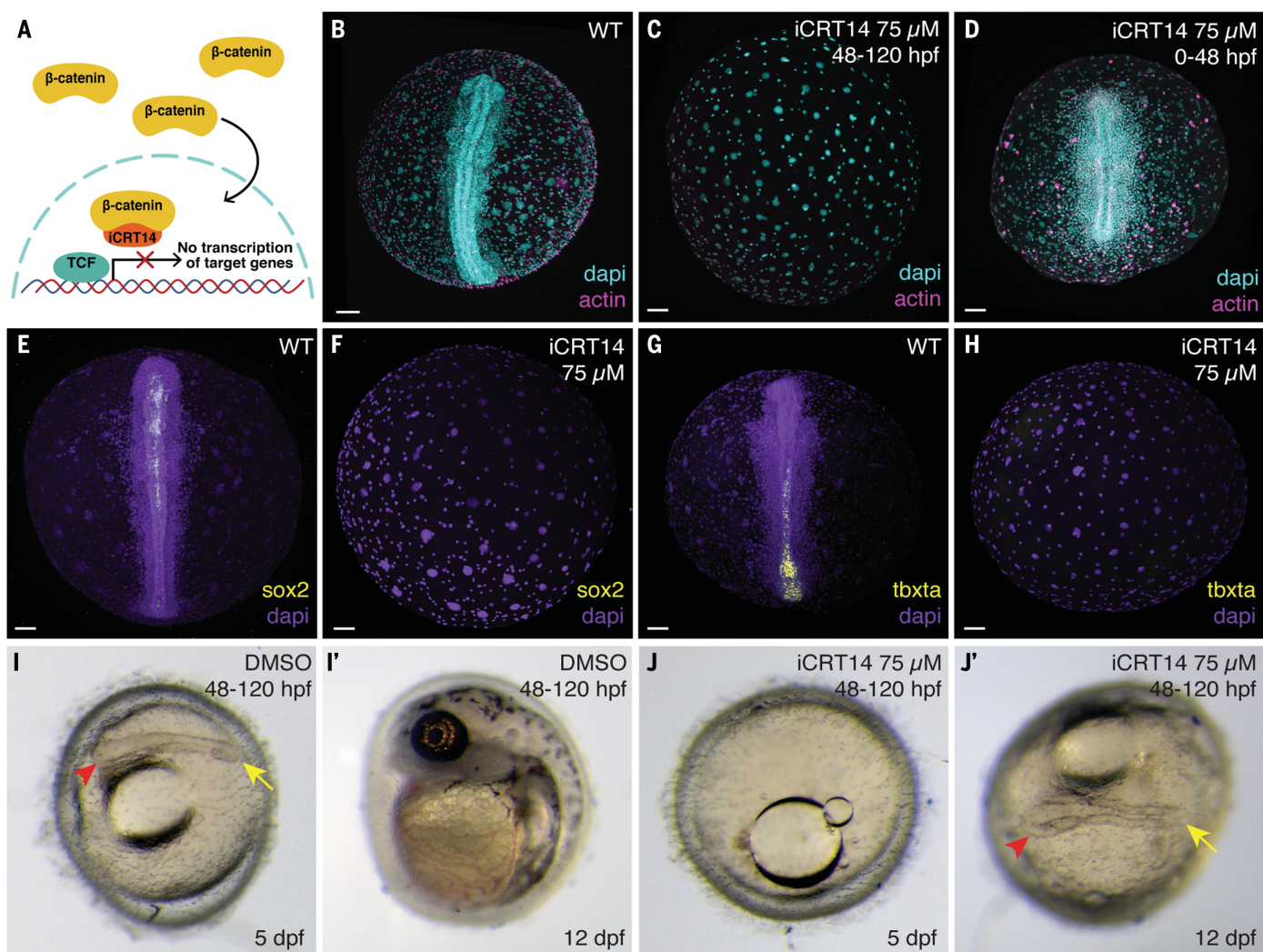


**Fig. 4.  $\beta$ -catenin is required for aggregation.** (A) Schematic showing the mechanism of iCRT14. (B) WT 10-somite stage embryo at day 5 (100% developed axes,  $n = 55$ ). (C)  $\beta$ -catenin signaling inhibited embryos incubated with 75  $\mu$ M of iCRT14 from the dispersed phase to day 5 (0% developed axes,  $n = 59$ ). (D)  $\beta$ -catenin signaling inhibited embryos incubated with 75  $\mu$ M of iCRT14 from the one-cell stage to the dispersed phase, then assayed at day 5 (84.32% developed axes,  $n = 56$ ). (E) Sox2 mRNA expression assayed at day 5. (F) Sox2 mRNA expression assayed at day 5 after incubation with 75  $\mu$ M of

iCRT14, starting from the dispersed phase. (G) *Tbxta* mRNA expression assayed at day 5. (H) *Tbxta* mRNA expression assayed at day 5 after incubation with 75  $\mu$ M of iCRT14, starting from the dispersed phase. Control embryo at day 5 (100% developed axes by day 5,  $n = 87$ ) (I) and day 12 (I') after incubation with 2% DMSO from the dispersed phase to day 5.  $\beta$ -catenin signaling inhibited embryo at day 5 (0% developed axes on day 5,  $n = 82$ ) (J) and day 12 (47.96% of embryos recovered by day 26,  $n = 82$ ) (J') after incubation with 75  $\mu$ M of iCRT14 from the dispersed phase to day 5. dpf, days postfertilization. Scale bars, 50  $\mu$ m.

state might be incompatible with prepatterning: First, it is conceivable that during diapause, cellular damage could accumulate and affect a prepatterned dorsal axis. Dispersion might serve as a buffer from this type of damage, allowing cells to aggregate using the remaining uncommitted cells (4, 28, 29). Second, the cellular rearrangements that occur during dispersion might erase maternal prepatterns due to the loss of prior spatial information. Indeed, dissociation and aggregation of zebrafish blastomeres can impede axis formation (30). Third, prolonged developmental arrest could flatten previously formed morphogen gradients (31). Thus, dispersion might facil-

itate survival during diapause but may preclude maternal prepatterning as a viable mechanism for axis formation. Indeed, blocking the interaction between  $\beta$ -catenin and TCF maintained cells in the dispersed phase and blocked specification. Notably, this developmental arrest was reversible once iCRT14 was washed out, resulting in axis formation days later (Fig. 4, I and J). It is tempting to speculate that  $\beta$ -catenin signaling might govern the decision to exit diapause I.

What is the relationship between the apparent self-organization of the *N. furzeri* aggregate and the embryonic patterning of other metazoans? Notably, human and mouse embryonic stem

cells can be induced to self-organize, express germ layer markers, and resemble gastrula stage embryos (32–35). Moreover, even species that normally prepattern their axes (e.g., sponges, anemone, and amphibians) have been shown to have the capacity to self-organize after experimental dissociation (36–38). These observations suggest that when challenged, some animals that normally prepattern their embryos may have the ability to pattern their axes through an alternative, self-organizing route. We speculate that in annual killifish, this self-organized route of development may have become fixed in order to survive the selective pressures imposed by their extreme environment.

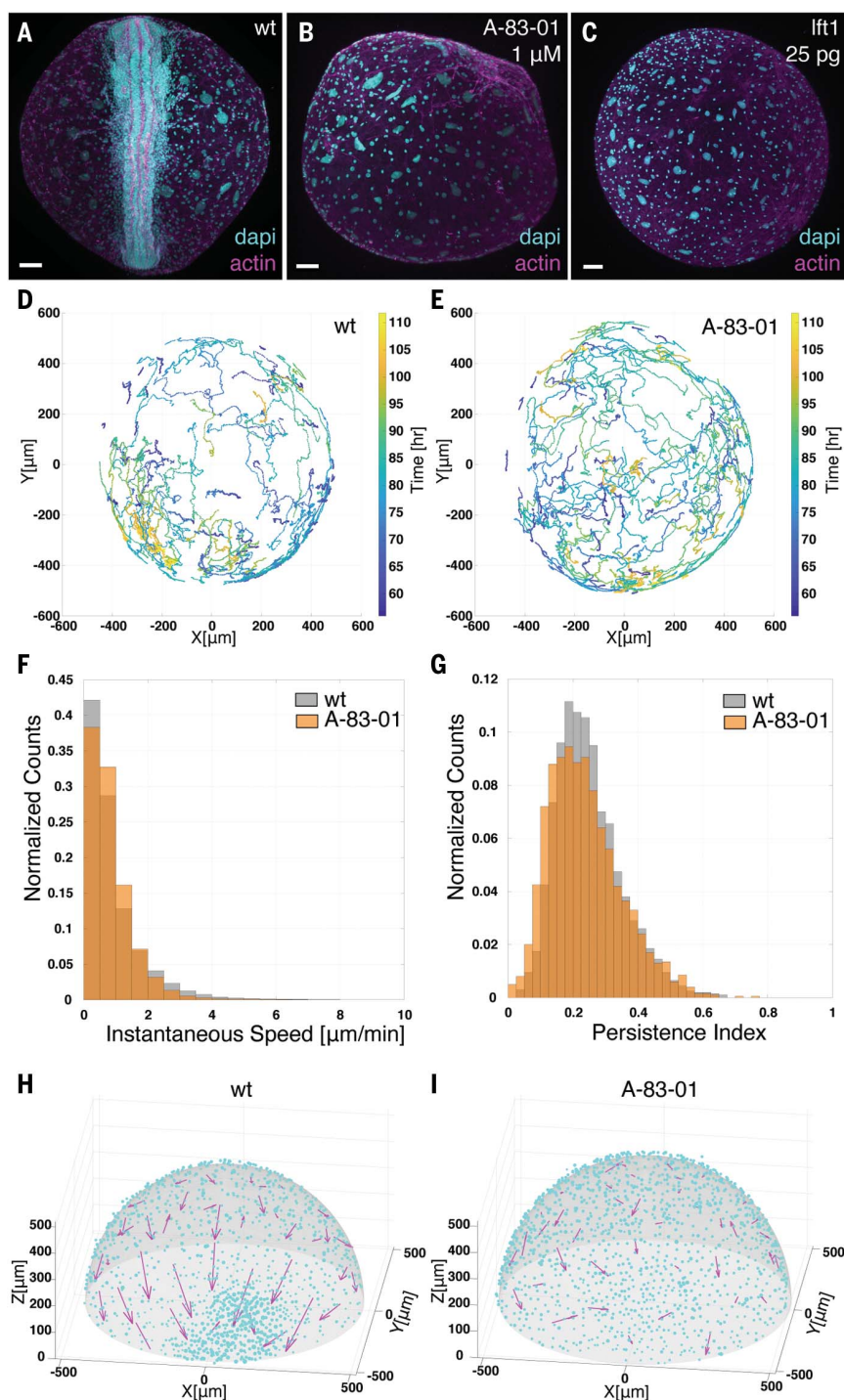


**Fig. 5. Nodal is required for coordinated morphogenesis.** (A) WT 10-somite stage embryo at day 5 (96.7% developed axes,  $n = 30$ ). (B) Nodal inhibited embryo incubated with 1  $\mu$ M A-83-01 from the dispersed phase to the incipient aggregate stage, then assayed at day 5 (0% developed axes,  $n = 43$ ). (C) Embryo injected with 25 pg of *lef1* mRNA at the one-cell stage, then assayed at day 5 (5.9% developed axes,  $n = 17$ ). (D) The top 200 cell trajectories with the most super-linear mean-squared displacement (MSD) curves from a timelapse of WT development between 50 and 110 hpf. (E) The top 200 cell trajectories with the most super-linear MSD curves from a timelapse of 2  $\mu$ M A-83-01 inhibited development between 50 and 110 hpf. (F) Distributions of instantaneous speeds in WT and A-83-01 inhibited embryos. (G) Distributions of persistence indices in WT and A-83-01 inhibited embryos. (H) Comparison of local cell-cell alignment in WT and (I) A-83-01 inhibited embryos from 72 to 108 hpf. Magenta arrows represent the direction and magnitude of the local alignment in each area bin. Cyan dots indicate the position of each cell at 108 hours. The aggregate is positioned at zero on the x axis, and approximately half of the volume of the embryo was imaged. Scale bars, 80  $\mu$ m in (A) to (C).

## REFERENCES AND NOTES

- H. Spemann, H. Mangold, *Int. J. Dev. Biol.* **45**, 13–38 (2001).
- L. Yan et al., *Science* **362**, eaat1045 (2018).
- A. F. Schier, W. S. Talbot, *Annu. Rev. Genet.* **39**, 561–613 (2005).
- J. P. Wourms, *J. Exp. Zool.* **182**, 169–200 (1972).
- G. Reig et al., *Nat. Commun.* **8**, 15431 (2017).
- L. Pereiro et al., *Dev. Dyn.* **246**, 812–826 (2017).
- T. Iwamatsu, *Mech. Dev.* **121**, 605–618 (2004).
- M. Poláček, R. Blažek, M. Reichard, *Nat. Protoc.* **11**, 1396–1413 (2016).
- D. R. Valenzano et al., *Cell* **163**, 1539–1554 (2015).
- C. N. Bedbrook, R. D. Nath, R. Nagarkar, K. Deisseroth, A. Brunet, *eLife* **12**, e80639 (2023).
- S. T. Dougan, R. M. Warga, D. A. Kane, A. F. Schier, W. S. Talbot, *Development* **130**, 1837–1851 (2003).
- S. Schneider, H. Steinbeisser, R. M. Warga, P. Hausen, *Mech. Dev.* **57**, 191–198 (1996).
- B. Traenkle et al., *Mol. Cell. Proteomics* **14**, 707–723 (2015).
- B. Feldman et al., *Nature* **395**, 181–185 (1998).
- Y. Okuda et al., *Dev. Dyn.* **235**, 811–825 (2006).
- M. Rhinn, K. Lun, M. Lutz, M. Werner, M. Brand, *Development* **132**, 1261–1272 (2005).
- M. C. Mullins et al., *Development* **123**, 81–93 (1996).
- F. C. Gonsalves et al., *Proc. Natl. Acad. Sci. U.S.A.* **108**, 5954–5963 (2011).
- J. M. Atkinson et al., *PLOS ONE* **10**, e0125028 (2015).
- M. Tojo et al., *Cancer Sci.* **96**, 791–800 (2005).
- K. McDole et al., *Cell* **175**, 859–876.e33 (2018).
- D. Soroldoni, B. Bajoghi, N. Aghaallaei, T. Czerny, *Gene Expr. Patterns* **7**, 93–101 (2007).
- G. Pézeron et al., *Curr. Biol.* **18**, 276–281 (2008).
- Z. Liu, S. Woo, O. D. Weiner, *Development* **145**, dev163535 (2018).
- M. L. Williams, L. Solnicka-Krezel, *eLife* **9**, e54445 (2020).
- A. Carmany-Rampey, A. F. Schier, *Curr. Biol.* **11**, 1261–1265 (2001).
- N. B. David, F. M. Rosa, *Development* **128**, 3937–3947 (2001).
- J. T. Wagner, J. E. Podrabsky, *Evodev* **6**, 2 (2015).
- C.-K. Hu et al., *Science* **367**, 870–874 (2020).
- A. Schauer, D. Pirheiro, R. Hauschild, C.-P. Heisenberg, *eLife* **9**, e55190 (2020).
- P. Müller, K. W. Rogers, S. R. Yu, M. Brand, A. F. Schier, *Development* **140**, 1621–1638 (2013).
- M. N. Shahbazi, E. D. Sigga, M. Zernicka-Goetz, *Science* **364**, 948–951 (2019).
- B. A. T. Weatherbee et al., *Nature* **622**, 584–593 (2023).
- B. Oldak et al., *Nature* **622**, 562–573 (2023).
- N. Moris et al., *Nature* **582**, 410–415 (2020).
- A. Kirillova et al., *Proc. Natl. Acad. Sci. U.S.A.* **115**, 1813–1818 (2018).
- P. D. Nieuwkoop, *Roux Arch. Dev. Biol.* **201**, 18–29 (1992).
- H. V. Wilson, *J. Exp. Zool.* **5**, 245–258 (1907).

## ACKNOWLEDGMENTS

We thank the following individuals: S. Sattler, N. Lord, A. Carte, A. Nichols, R. Losick, and Y. Wan for helpful discussions and critical reading of the manuscript; K. McDole for providing advice about automated cell tracking; C.-K. Hu for providing embryos and training; B. Hughes, J. Miller, K. Hurley, K. Berg, and T. Kimura for animal husbandry; D. Richardson of the Harvard Center for Biological Imaging for microscopy support; J. Sohn for helpful discussions; and R. Losick for generous hospitality. **Funding:** P.B.A. was supported by a Damon Runyon Postdoctoral Research Fellowship and Searle Scholars Program. D.C.A. was supported by a graduate fellowship from the US National Science Foundation and the Molecular Biophysics Training Grant (PI: J. M. Hogle, NIH/NIGMS T32 GM008313). This work was supported by a grant from the US National Institutes of Health (5R37GM056211), an ERC Advanced Grant and the Allen Discovery Center for Cell Lineage Tracing. **Author contributions:** P.B.A. and A.F.S. conceived the study. P.B.A., L.M.S., D.C.A., and A.F.S. interpreted results and wrote the paper. P.B.A. and L.M.S. designed and performed all experiments. D.C.A. analyzed the light sheet data. **Competing interests:** Authors declare no competing interests. **Data and materials availability:** All data are available in the manuscript or supplementary materials. **License information:** Copyright © 2024 the authors, some rights reserved; exclusive licensee American Association for the Advancement of Science. No claim to original US government works. <https://www.science.org/about/science-licenses-journal-article-reuse>

## SUPPLEMENTARY MATERIALS

[science.org/doi/10.1126/science.ado7604](https://science.org/doi/10.1126/science.ado7604)

Materials and Methods

Figs. S1 to S8

References (39–45)

MDAR Reproducibility Checklist

Movies S1 to S5

Submitted 19 February 2024; accepted 8 May 2024  
10.1126/science.ado7604